Bull Earthquake Eng (2013) 11:687–707
DOI 10.1007/s10518-012-9393-4

ORIGINAL RESEARCH PAPER

Finite element analysis and experimental verification of the scrap tire rubber pad isolator

Huma Kanta Mishra · Akira Igarashi · Hiroshi Matsushima

Received: 6 March 2012 / Accepted: 15 October 2012 / Published online: 31 October 2012

Abstract A new base isolation system using scrap tire rubber pads (STRP) has been introduced for seismic mitigation of ordinary residential buildings. The rubber and the steel reinforcing cords used in manufacturing the tire are the alternative materials of the proposed base isolation system. The steel reinforcing cords represent the steel plates used in conventional laminated rubber bearings. These steel reinforcing cords shall prevent the lateral bulging of the rubber bearing. The proposed base isolation system has no bonding between the superstructure and the foundation beam which allows for rollover deformation. In the first part of the study, the STRP layers were just stacked one on top of another without applying the adhesive. This paper presents loading test as well as finite element analysis (FE analysis) of strip STRP isolators that are subjected to any given combination of static vertical and lateral loads. The results of the static vertical and horizontal loading test conducted on STRP isolators were used to calculate the mechanical properties of the isolators, including stiffness and damping values. The load–displacement relationship of STRP isolators were compared between experimental and FE analysis results and the results were found to be in close agreement. The stress state within the STRP isolators was also analyzed in order to estimate the maximum stress demand in the rubber and steel reinforcing cords. These STRP isolators have several advantages over conventional laminated rubber bearings including superior damping properties, lower incurred cost, light weight and easily available material. This study suggests that using the STRP as low cost base isolation device for ordinary residential buildings is feasible.

H. K. Mishra (✉)
Department of Urban Management, Kyoto University, Kyoto, Japan
e-mail: h.mishra@kt3.ecs.kyoto-u.ac.jp

A. Igarashi · H. Matsushima
Department of Civil and Earth Resources Engineering, Kyoto University, Kyoto, Japan
e-mail: igarashi.akira.7m@kyoto-u.ac.jp

H. Matsushima
e-mail: hiroshi.m@hs7.ecs.kyoto-u.ac.jp

Keywords STRP isolators · Laminated rubber bearings · Finite element analysis · Low cost base isolation · Uniaxial tension test

1 Introduction

Past earthquakes in developing countries have underlined particular vulnerability of poorly constructed masonry as well as reinforced concrete structures (Kelly 2002a,b). Improper design methods, poor quality construction materials, and inadequate supervision are the key factors in creating the vulnerability of structures. Masonry structures have low ductility and brittle structural components that are the reasons for severe damage during the earthquake events. These damages cause huge amount of property loss and increase loss of lives even when a medium earthquake occurs. In order to enhance resistance of masonry structures against earthquake forces, design methods based on increasing strength using reinforced masonry and reinforced concrete ties are incorporated in various codes (Tomažavič et al. 2009). However, these masonry structures can still be cracked or damaged during strong earthquakes.

The conventional seismic design approach in recent practices is aimed to provide adequate strength and ductility in order to maintain the structural integrity and to absorb seismic energy. This method is based on the fact that the structural components have to be designed for the required seismic demand. If the level of seismic demand on these structures were reduced through a simple but reliable engineering solution, this would result in fewer building failures and decreased loss of lives during the past earthquakes (Toopchi-Nezhad et al. 2008).

The technique known as the base isolation is used to reduce the seismic demand instead of increasing the earthquake resistant capacity of the structures. Application of this technology in developed countries is limited to the important and valuable structures. The reason behind this is the size, weight and incurred cost. It is straightforward that commercially available base isolation devices are far from the reach of a poor family in developing countries. A reduction in the weight and cost of elastomeric seismic isolators would permit a significant increase in their application to many ordinary residential and commercial buildings (Toopchi-Nezhad et al. 2008).

Few studies have been conducted using either steel laminated rubber bearing (Kelly and Konstantinidis 2007) or fiber-reinforced elastomeric isolators (Kelly 2002a,b; Toopchi-Nezhad et al. 2008; Mordini and Strauss 2008) as low cost base isolation systems for highly seismic regions of the world. These types of seismic isolators are still economically unacceptable considering the purchasing capacity of poor families in the South Asian region. The solution of the above issues shall be the development of base isolation systems which can be effective in reducing the seismic demand of the structures and are made of easily available materials at an affordable cost.

A new type of seismic isolation system has been introduced using the scrap tire rubber as easily available material at low or negligible cost. The research on scrap tire pad has been initiated by Turer and Özden (2008), in which the researchers produced the specimen samples using car tires and tested in vertical compression and in horizontal shear. The experimental test was conducted only stacking the samples one on top of another. The car tire usually contents synthetic fiber as reinforcing cords. Due to this reason, Turer et al. have mentioned that the scrap tire pad sample begins failure in compression at about 8.5 MPa axial stress. This result appears to show that the examined

STRP isolators were insufficient for the practical use of scrap tire rubber pad in building isolation.

In this study, either the scrap tires of bus or truck are used to produce the specimen samples. Only the rubber from the tread section of the scrap tire was used. In first part of the study, the STRP layers were just stacked one on top of another without applying the adhesive. These isolators were not bonded between the superstructure and substructure so that rollover deformation is allowed. This rollover deformation decreases the effective stiffness of the isolator during the increase in lateral displacement which further increases the efficiency of the isolation system provided that stability is achieved (Toopchi-Nezhad et al. 2011). An additional advantage of the STRP isolator compared to the conventional steel laminated rubber bearing is that, the STRP bearing can be placed closely in case of masonry building structures.

In this paper, the results of experimental tests and finite element analysis (FE analysis) conducted on unbonded square STRP isolators are presented to investigate the performance of STRP isolators. The hyperelastic material constants used in FE analysis were derived by conducting uniaxial tension test of dumbbell shape rubber samples. The experimental data fit technique was employed in order to determine the representative material constants, although these material constants are generally derived by using the different deformational modes namely; uniaxial tension test, equibiaxial tension test and planar shear test. The experimental test results were used to compute the mechanical properties of the STRP-6 isolator including stiffness and damping values. Furthermore, stiffness of the isolators was computed using the established relationship and compared with the result of FE analysis. These results were further compared with relevant code provisions (UBC 1997; Eurocode 8 2004; ASCE 2005) to check whether the STRP isolators can be used as base isolation device or not. The results of FE analysis also provide the information about stress state and strain state within the STRP isolator.

2 Scrap tire rubber pad

Several samples of STRP isolators as shown in Fig. 2b were designed and prepared for testing in compression and shear. Following steps describe the procedure of specimen sample preparation.

1. The specimen samples were prepared by using recently scrap bus or truck tires
2. The STRP samples were prepared by companies specialized in tire re-processing for re-treading. This process is mechanized in Japan for the reprocessing of tires. Similar methodology can be adopted to produce the STRP isolators in developing countries. First of all, uneven part of the tread section was removed to make plain and smooth surface.
3. Both of the side walls of the tire was cut and removed and a long rectangular strip type specimen was prepared. Only the rubber along the tread part was used for the production of STRP bearings.
4. This rectangular strip type belt was cut to the required size as per design of rubber bearings. Since the maximum width of a bus/truck tire was found to be 162–240 mm, production of small to sufficiently large size rubber bearings is possible.
5. Stacking of these small strips in different orientations for alternative layers can produce even larger size of rubber bearings as per the requirements. The required thickness of rubber bearings were obtained by stacking one on top of the other in vertical layers.

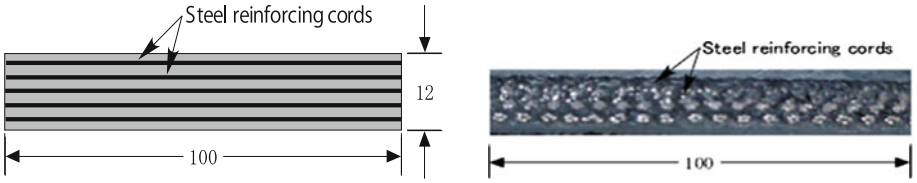

Fig. 1 Cross section of single layer STRP sketch and photograph

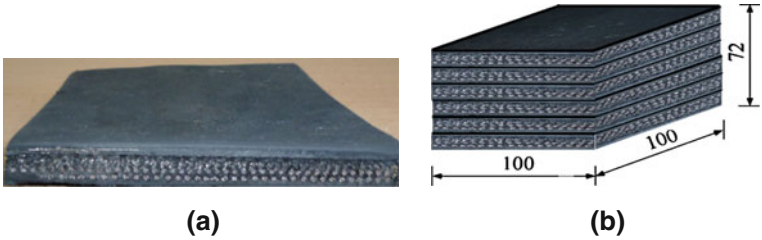

Fig. 2 Photograph of STRP samples (dimensions are in mm). **a** Single layer STRP, **b** six layers STRP isolator

Table 1 Assumed material and geometrical properties of STRP isolator

Material properties	Geometrical properties
Shear modulus of rubber $G = 0.89$ MPa	Width of the STRP = 100 mm
Poisson's ration of steel cords $\nu = 0.3$	Thickness of a single layer STRP = 12 mm
Young's modulus of steel cords E = 200 GPa	Thickness of steel reinforcing cords = 0.4 mm
	Total thickness of STRP-6 = 72 mm, tr = 60 mm

6. The original designed size of the STRP isolators was different from those used in the experimental testing due to the capacity of the testing equipment available. Two STRP samples were prepared.

Each layer of STRP isolator contains five layers of steel cords interleaved and bonded between the layers of rubber as shown in Fig. 1. These steel reinforcing cords comprise a number of strands in a twisted form. The photograph including the dimensions of the STRP-6 isolator is shown in Fig. 2b and the geometrical and material properties are given in Table 1.

3 Experimental set up and testing procedure

Figure 3a shows a sketch of the test setup to perform the vertical and horizontal tests. The STRP-6 isolator was placed between the upper and lower steel plate surfaces of the loading test setup as shown in the photograph in Fig. 3b. The vertical load was applied to the specimen by the vertical hydraulic actuator through a stiff frame mounted on the floor and the reaction wall. The vertical hydraulic actuator had a maximum loading capacity of ±400 kN and maximum displacement capacity of ±50 mm in the vertical direction. The horizontal load was applied to the same frame with the horizontal actuator. The test machine had a maximum displacement capacity of ±125 mm and a maximum loading capacity of ±400 kN in the horizontal direction. The capacity of the testing facility is also presented in Table 2. Two sets of tests for STRP-6 samples were conducted.

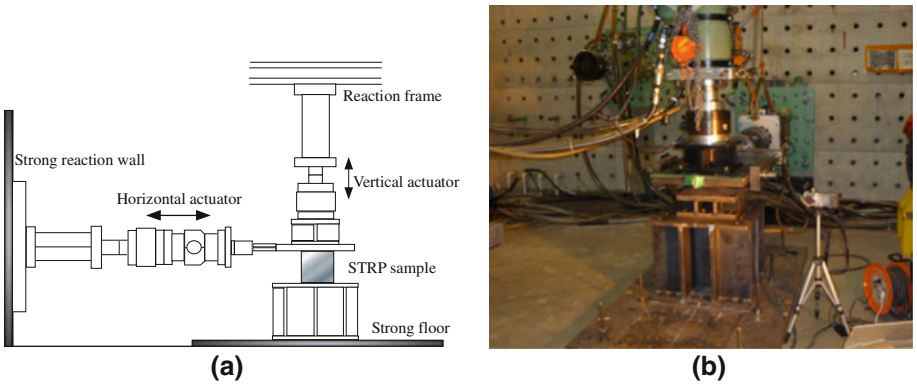

Fig. 3 Overview of test setup and instrumentation arrangement. **a** Sketch, **b** photograph

Table 2 Capacity of testing facility

Actuator	Max. displacement (mm)	Max. load (kN)	Remarks
No. 1	±125	±400	Horizontal
No. 2	±50	±400	Vertical

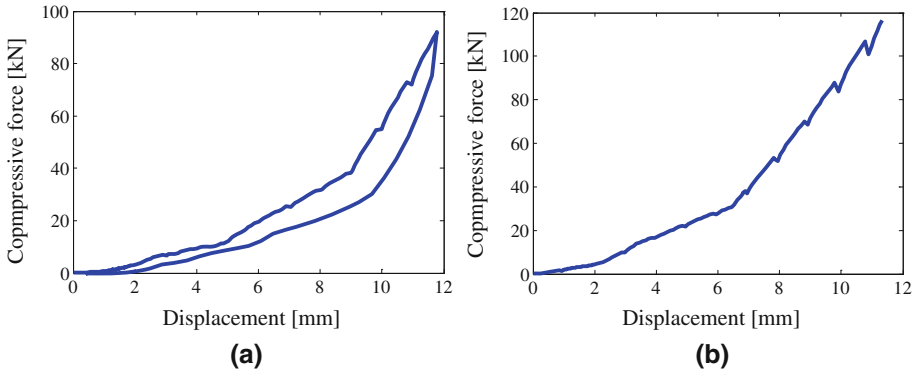

Fig. 4 Vertical load–deflection relationships of STRP-6. **a** 91.9 kN compressive load, **b** 116.6 kN compressive load

3.1 Compression test

The compression modulus as well as the maximum vertical deflection of the specimen was evaluated through vertical compression testing. The STRP-6 specimen samples were tested under vertical displacement control. The first specimen was monotonically loaded to 12 mm vertical displacement which resulted in the equivalent vertical force of 91.9 kN and is equivalent to 9.19 MPa vertical pressure on the STRP-6 sample. In the final stage of the vertical testing, the specimen was monotonically unloaded. Displacement was increased by 1 mm within the 10 s interval. A similar test at an equivalent of 11.66 MPa vertical pressure was performed using the second sample to study the vertical stiffness at a higher value of vertical load. In the latter case, unloading was not performed, as shown in Fig. 4b. The vertical stiffness of the isolators was calculated using the load deflection relationship shown in

Fig. 5 Input signal

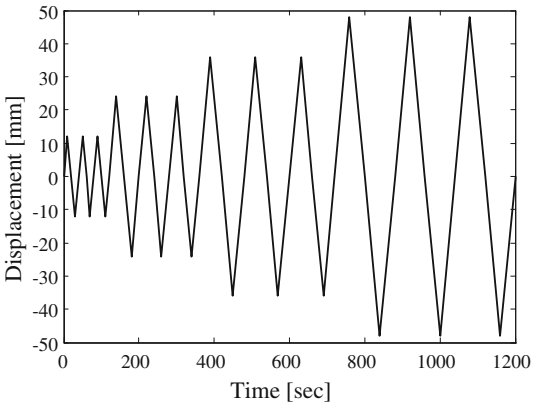

Fig. 6 Force–displacement relationship

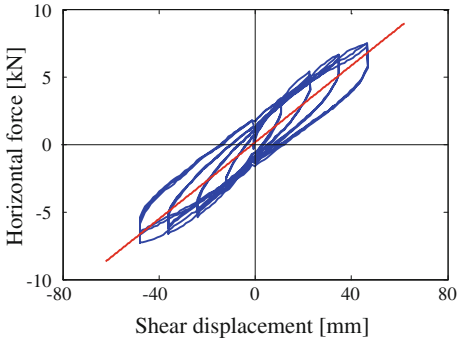

Fig. 4. From the test results, the vertical stiffness values described above were calculated as $(K_V)_1 = 21{,}598.87\,\text{kN/m}$ and $(K_V)_2 = 20{,}699.35\,\text{kN/m}$, respectively. These values correspond to effective compression moduli of $E_1 = 155.51\,\text{MPa}$ and $E_2 = 149.03\,\text{MPa}$.

3.2 Cyclic shear test

The cyclic shear test on the isolators provides the reliable methods to determine the deformation characteristics and damping values of isolation systems. The static shear test was performed under horizontal displacement control. The STRP-6 specimen was tested in cyclic shear with three fully reversed cycles at four maximum shear displacement amplitudes of 12, 24, 36, and 48 mm. The loading history in the horizontal shear test is presented in Fig. 5 and corresponding force-displacement relationship in cyclic shear is shown in Fig. 6. These cycles were applied at a constant vertical pressure of 5 MPa.

3.3 Monotonic shear test

The purpose of the monotonic shear test was to evaluate the maximum shear deformation capacity of the unbonded STRP-6 isolator and residual slip if it exists. The specimen sample was tested at six maximum shear displacement amplitudes of 12, 24, 36, 48, 60, and 62 mm. The loading history in the static monotonic shear test is shown in Fig. 7 and corresponding force-displacement relationship in monotonic shear is shown in Fig. 8. These displacement amplitude cycles were applied at a constant vertical pressure of 5 MPa. At the end of the max-

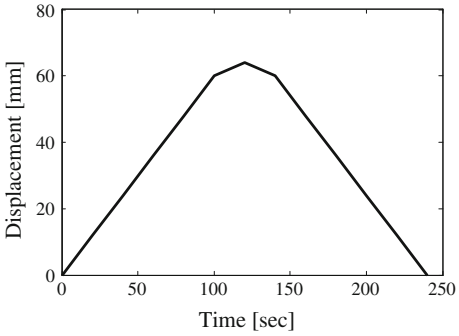

Fig. 7 Input signal

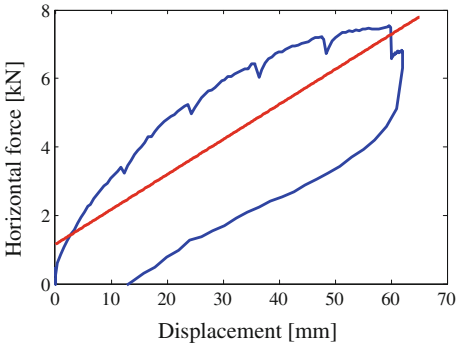

Fig. 8 Force–displacement relationship

Fig. 9 Deformed state of STRP-6 under constant 5 MPa vertical pressure. **a** 80 % shear strain, **b** 103 % shear strain

imum lateral displacement, gradual unloading was performed. During the complete experimental testing, no residual slip was observed. The deformed state of STRP-6 isolator under constant 5MPa vertical pressure is shown in Fig. 9.

Table 3 Horizontal stiffness of STRP isolator

Test no.	Sample	Size of sample	Horizontal displacement (mm)	Horizontal stiffness (kN/m)
1	STRP-6	100 × 100 × 72	48	142.48
2	STRP-6	100 × 100 × 72	62	102.20

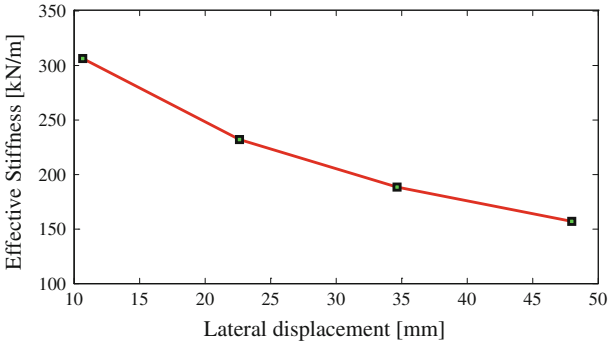

Fig. 10 Relationship between effective stiffness and lateral displacement

4 Horizontal stiffness of STRP isolator

The isolator's effective horizontal stiffness corresponding to each load cycle of the test can be calculated based on the peak lateral loads and the peak lateral displacements as follows (UBC 1997):

$$K_{eff} = \frac{F^+ - F^-}{\Delta^+ - \Delta^+} \tag{1}$$

where F^+, F^-, Δ^+, and Δ^- are the peak values of horizontal load and horizontal displacement, respectively, at the positive and negative sign extremes of the cyclic displacement range. For the last cycle of the test, the effective horizontal stiffness of the first sample is 156.63 kN/m. The average horizontal stiffness of the STRP isolators was evaluated using the least-square fitting technique. Theoretical horizontal stiffness of the STRP-6 isolator is calculated using the conventional and established relationship. The maximum lateral displacements as well as the horizontal stiffness values of the STRP isolators are presented in Table 3.

The results of the experimental test were used to calculate the effective horizontal stiffness at shear displacement amplitudes of 12, 24, 36 and 48 mm and are shown in Fig. 10. Due to the rollover deformation, the effective horizontal stiffness decreases with increase in lateral displacement which would further elongates the natural period of the system.

5 Effective damping in STRP isolator

The effective damping (β_{eff}) of an isolator shall be calculated for each cycle of loading by the formula (UBC 1997):

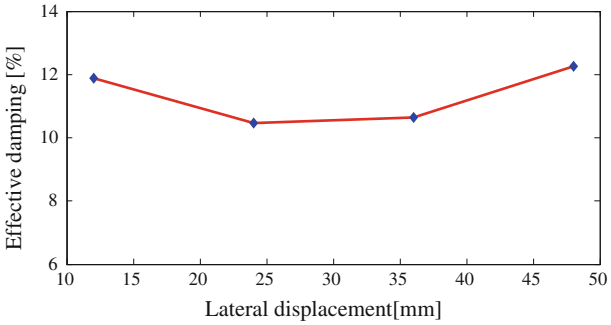

Fig. 11 Relationship between effective damping and lateral displacement

$$\beta_{eff} = \frac{2}{\pi}\left[\frac{E_{Loop}}{K_{eff}\left(\left|\Delta^{+}\right| + \left|\Delta^{-}\right|\right)^{2}}\right] \tag{2}$$

where E_{Loop} is the energy dissipated per cycle of the loading, K_{eff} is the effective horizontal stiffness.

The computed damping ratio represents the damping of the whole cord–rubber composite. It was found that the damping ratio is highly dependent on pre-loading (Mishra and Igarashi 2012), as also shown by the study carried out by Gerhaher et al. (2011). Although it is known that the effective damping can also be dependent on the frequency and vertical axial load, the results shown are for the condition of quasi-static loading, and a constant normal pressure of 5 MPa.

These values are in a close agreement with the value obtained in the previous study (Turer and Özden 2008). The effective damping value is higher than that of the low damping natural rubber bearings which is reported as 2–3 % damping (Naeim and Kelly 1999). The relationship between lateral displacement and effective damping values is shown in Fig. 11 for the entire range of lateral displacement.

The steel reinforcing cords are more flexible in tension than the individual filaments; therefore, they may stretch when the STRP bearing is loaded by the weight of a structure. On the other hand, they are completely flexible in bending, implying that the assumption for modeling steel laminated rubber bearing that plane sections remains plane after loading no longer holds (Kelly 1999). In fact, when a STRP bearing is loaded in shear, a plane cross section is distorted. This leads to additional advantage in the use of STRP isolators having steel reinforcing cords, when the bearing is deformed in shear, the tension in the cord strand produces a frictional damping that is due to individual filaments in the strand slipping against each other. This energy dissipation in the steel reinforcing cords is added to that of the rubber. The STRP-6 specimen test shows that this energy dissipation is much larger than that of rubber (12 % damping at 80 % shear deformation). Therefore, when using STRP isolator for a specified level of damping, use of an additional damping enhancement mechanism can be avoided.

6 Finite element analysis

The FE analysis of the strip STRP-6 isolator was carried out in order to access the force–displacement relationship and evaluate the stress state within the isolator. Although shear deformation capacity of the STRP isolator cannot be expected as much as steel laminated rubber bearings, a properly bonded STRP isolator is expected to have more than 150 % shear

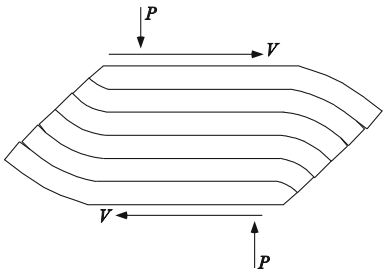

Fig. 12 Free body diagram of laterally deformed STRP isolator

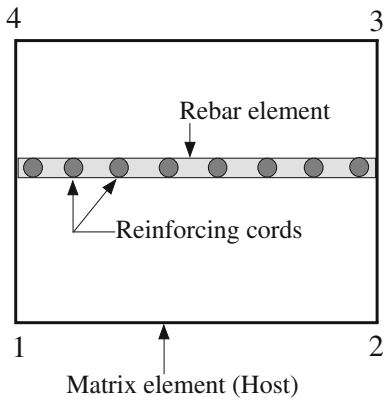

Fig. 13 Rebar and rubber element

deformation capacity. The sketch of the deformation pattern of the unbonded STRP isolator is shown in Fig. 12. The moment created by the offset of the resultant compressive force P balances the moment created by the shear force V. Due to this reason, no tension stresses are produced within the STRP isolator.

6.1 Modeling of STRP isolator

The STRP that constitutes the isolator is composed of a rubber body with embedded steel reinforcing cords. The isolator's physical and geometrical properties are given in Table 1. FE analysis of the strip STRP was conducted using a commercially available general purpose finite element software (MSC Software 2010). The rubber was modeled using four-node, isoparametric quadrilateral elements coded for plane strain incompressible applications. This element is preferred over higher-order elements when used in simulating large deformation and contact analysis (MSC Volume A 2010). The reinforcing steel cords were modeled by using the isoparametric plane strain two-node line elements. These elements need to be used in conjunction with four-node plain strain continuum elements (host elements). These rebar elements have to be embedded into their corresponding solid elements representing the matrix materials. The typical rebar element inserted into the rubber element is shown in Fig. 13. Since the matrix element and the rebar element share the same nodal points, no additional degrees of freedom are introduced. Marc automatically ties the degree of freedom of the nodes to be inserted to the corresponding degree of freedom of the host elements. The rebar model allows that the rubber and the steel reinforcing cords are described by different stress–strain constitutive relationships. When defining the material properties of the rebar layer, the reference plane or the edge of the rebar layer should be defined. In this model, the

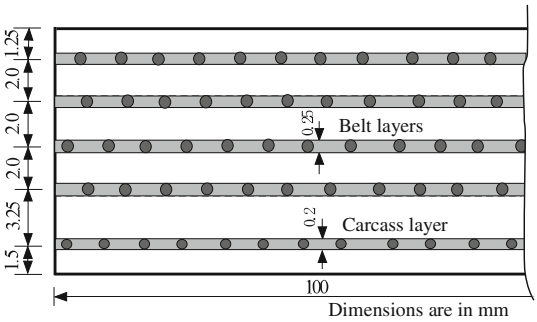

Fig. 14 Steel reinforcing cords in a single layer STRP

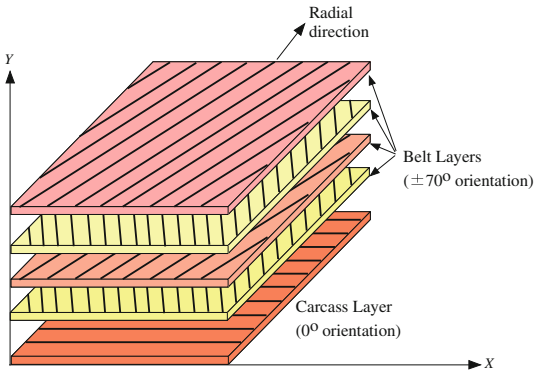

Fig. 15 Layout of steel reinforcing cords

reference axis of rebar direction, the cross-section area of a single rebar, density/spacing of the rebar, angle of orientation with respect to the reference axis has to be defined.

Figure 14 shows the dimensions of a single layer STRP used in preparing the finite element model. In this figure, the indicated thickness of a layer is the equivalent thickness defined by the total area of reinforcing cords divided by the width of the isolator. For the top and bottom layers, the edge length of the quadrilateral elements was selected to be approximately 0.4 mm, while that for the intermediate layers is approximately 0.5 mm. These modeling techniques were also used to model the steel reinforcing cords. The 2D finite element model adopts quadrilateral and line elements. There are 8,750 quadrilateral elements and 1,250 rebar elements in a single layer of STRP placed near the uppermost and lowermost support surfaces. The number of quadrilateral and rebar elements in the middle layers was reduced to 5,800 and 1,000, respectively. There are total of 47,200 elements in a STRP-6 isolator. The area of a single steel reinforcing cord in the carcass layer is 0.44 mm^2, while in the belt layer is 0.63 mm^2. The spacing of the steel reinforcing cords is about 0.4/mm. The orientation of the steel reinforcing cords were measured and verified by relevant literature (Wong 2001). The orientation of the individual layers with respect to the direction of the cords in the carcass layer is shown in Fig. 15. The orientation of the rebar direction was assigned as $\pm 70°$ for the belt layers about the reference axis. The typical finite element meshing for a single layer STRP is shown in Fig. 16. The rubber is modeled by a hyperelastic material model while the steel reinforcing cord in the finite element model is treated as a linear elastic isotropic material with material properties given in Table 1.

Two horizontal rigid bodies (lines) were defined at the top and bottom of the STRP isolator to represent the superstructure and substructure, respectively. In this model, the vertical

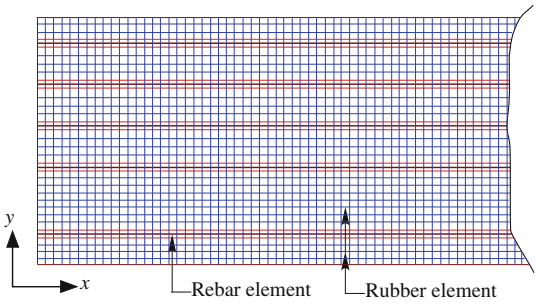

Fig. 16 Typical finite element mesh

and horizontal loads were applied on the top support; the top support was allowed to move in vertical and in horizontal directions while the bottom support was considered as a fixed support. These boundary conditions were exactly similar as were in the experimental testing. In this contact model, the contact between the supports and the STRP isolator was modeled by the Coulomb friction law with a coefficient of friction of 0.8. The coefficient of friction was selected such that no slips occur between the contact support and the rubber. The contact between the STRP layers was considered as a touching contact. The individual STRP layers were modeled as deformable bodies with a local coefficient of friction as 0.95. The STRP isolator was not bonded to the top and bottom support and its rollover deformation was allowed. This means that when the compression contact stresses approach to zero, the nodal points were allowed to detach from the contact supports.

Generally, rubber material is thought to be an isotropic hyperelastic material. Due to this reason, the mechanics of behavior of rubber can be described in terms of the strain energy density function. Among the various constitutive models, the Mooney–Rivlin model is commonly used to characterize the rubber material undergoing large strain (Ali et al. 2010). This model is simplest hyperelastic model for elastomeric materials when material test data is insufficient. The Mooney–Rivlin material law is well suited for most practical applications involving cord-reinforced rubber material (Helnwein et al. 1993). This material model works with incompressible elastomer and strains up to 200 %. The strain energy polynomial is expressed as:

$$W = \sum_{i,j=0}^{N} C_{ij} \, (I_1 - 3)^i \, (I_2 - 3)^j + \sum_{i=1}^{N} \frac{1}{D_i} \, (J_{el} - 1)^{2i} \tag{3}$$

where C_{ij} and D_i are material parameters that are found from test data, J_{el} is the elastic volume ratio, I_1 and I_2 are invariants of the green deformation tensor given in terms of principle stretch ratios. In Eq. (3), the first summation is the contribution due to deviatoric effects and the second summation is the contribution due to volumetric effects. The deviatoric contribution to the strain energy density function is (MSC Volume A 2010):

$$W = C_{10} \, (I_1 - 3) + C_{01} \, (I_2 - 3) + \cdots \tag{4}$$

where C_{10}, and C_{01} are the material constants known as the Mooney–Rivlin material constants. These material constants were evaluated by conducting uniaxial tension tests as discussed in the following sections.

6.2 Rubber material properties

The uniaxial tension tests were carried out up to engineering tensile strains of 4.36. The uniaxial tension test is usually conducted until tension failure of the material sample, in order to ensure that the strain energy function would adequately represent the relationship between engineering stresses and strains to validate the material model utilized in the FE analysis. In Eq. (4), the strain invariants are given by:

$$I_1 = \lambda_1^2 + \lambda_2^2 + \lambda_3^2 \tag{5}$$

$$I_2 = \lambda_1^2\lambda_2^2 + \lambda_2^2\lambda_3^2 + \lambda_3^2\lambda_1^2 \tag{6}$$

where λ_1, λ_2 and λ_3 are the stretch ratios in the principal directions, I_1 and I_2 are the first and second invariants of the strain tensor, respectively. Although the material constants $C_{10}, C_{01}, C_{11}, \ldots$ can be easily determined for the linear relationship either using uniaxial tension or compression test results, determination of the material constants is complicated for the nonlinear relationship. The model designated by Eq. (4) contains only two material constants, so that the model is simple (Vossoughi 1995). As reported, these material constants can be evaluated from a simple test such as uniaxial tension test with minimum numbers of measurements such as axial stress and axial strain, using the first order truncation of Eq. (3).

6.3 Specimen sample

For uniaxial tension tests, the specimen samples of uniform thickness of 2.0 mm were prepared by using scrap bus/truck tires to prepare the dumbbell specimen samples as per the Japanese Industrial standards (JIS) as shown in Fig. 17. The photograph of dumbbell specimen is shown in Fig. 18.

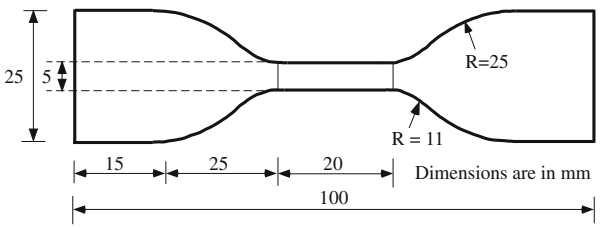

Fig. 17 Specimen sample for uniaxial tension test

Fig. 18 Photograph of dumbbell specimen sample

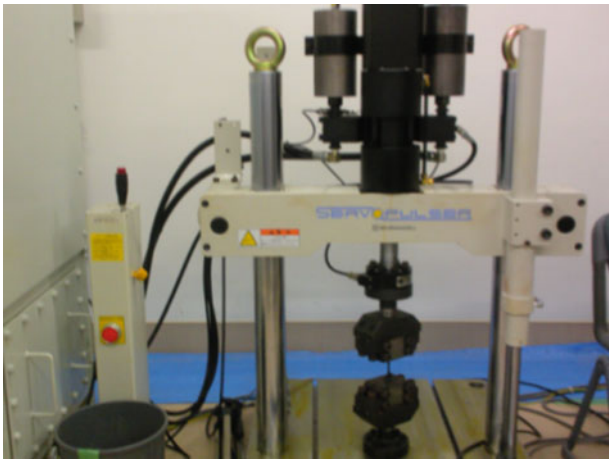

Fig. 19 Uniaxial tension test

6.3.1 Experimental setup and test

Dimensions of all the specimens prepared for the uniaxial tension test were measured before testing. The difference between the maximum and minimum thickness was less than 0.10 mm for each specimen. The equipment used in the experiment was a universal tensile test machine shown in Fig 19. A total of four samples were tested; three in monotonic tension and one in cyclic tension. A dumbbell shape specimen was tested in cyclic tension with single reversed cycle at four maximum extension amplitudes of 25, 50, 75, and 100 mm. In all the tests, the constant rate of extension at 1 mm/s was maintained. All the specimen samples were tested until their failure state.

The hyperelastic material constants expressed by Eq. (4) were derived by using least-square fitting procedure. Initially, all the experimental tests data were adjusted so that the curve passes through the origin. Secondly, the data were fitted using the least-square fit procedure which minimizes the sum of squared error between the experimental and calculated stress values. Mathematically, the relative least squared error can be expressed by:

$$error = \sum_{i=1}^{N} \left(1 - \frac{\sigma_i^{cal}}{\sigma_i^{\exp}}\right)^2 \tag{7}$$

where N is the total number of data points, σ_i^{cal} and $\sigma_i^{\exp}$ are the calculated and experimental stresses, respectively. To minimize the residual of the least squared error, a higher order Mooney–Rivlin strain energy polynomial was utilized. In this case, three-term Mooney–Rivlin material model was found to show close agreement with the experimental data fitting as shown in Fig. 21a, b. These constants were determined for the individual data set. The presented constants in Table 4 are the average of all the data sets which were used for modeling the STRP isolator.

6.3.2 Finite element analysis of dumbbell specimen

The purpose of the FE analysis is to derive the stress–strain relationship for different extension levels of the dumbbell specimen. These types of data are usually required to be compared with

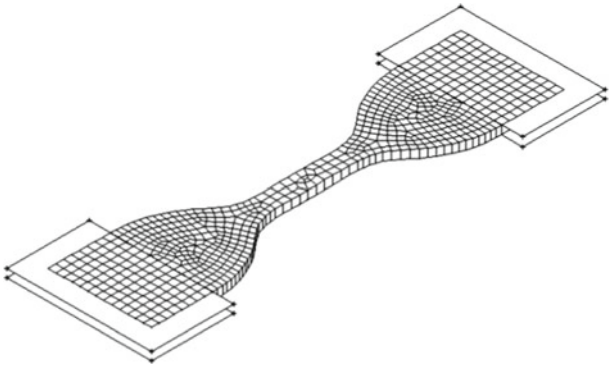

Fig. 20 Finite element model of dumbbell specimen

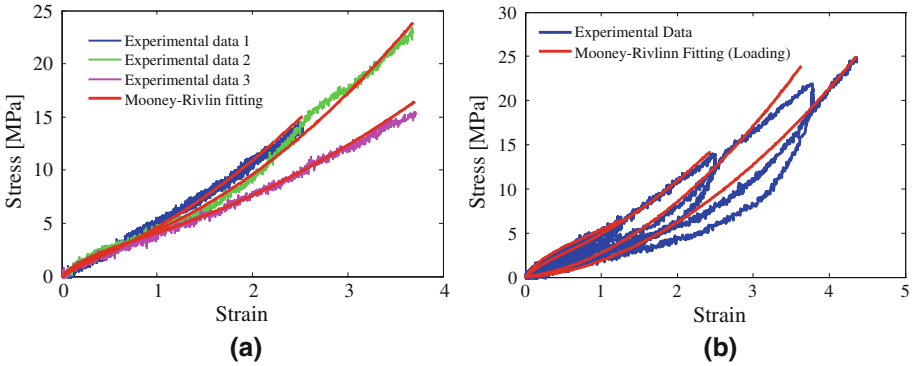

Fig. 21 Experimental data with Mooney–Rivlin curve fitting. **a** Monotonic uniaxial tension test, **b** cyclic uniaxial tension test

that of the data obtained from the uniaxial experimental test. The FE analysis of the dumbbell shape tire rubber specimen sample was carried out in order to assess the uniaxial stress–strain relationship. Three-dimensional finite element model of dumbbell shape specimen is shown in Fig. 20.

6.3.3 Modeling of dumbbell specimen

The simulated dumbbell specimen's dimensions are shown in Fig. 17. The rubber was modeled using eight-node three-dimensional isoparametric arbitrary elements for incompressible applications with Herrmann formulation (MSC Volume B 2010) since this element is preferred over higher-order element when used in simulating large deformation. The grip of the loading system is represented by two rigid surfaces on both ends of the specimen. In order to avoid the convergence problem and to effectively simulate the specimen, adaptive stepping technique was used.

6.3.4 Results and discussion

The results of the uniaxial tension test and FE analysis of the dumbbell specimens were compared in terms of the stress–strain curve. The average values of the entire specimen samples

Table 4 Mooney–Rivlin material constants

Rubber material properties	$C_{10} = 0.40000\,\text{MPa}$
	$C_{01} = 1.22315\,\text{MPa}$
	$C_{11} = 0.18759\,\text{MPa}$

were calculated to represent the overall Mooney–Rivlin material constants. These material constants were then used in the FE analysis of the STRP isolator and good correlation between the finite element and experimental test results were confirmed.

6.4 Loads

To investigate the nonlinear behavior of the STRP isolator, load was applied in an incremental manner. At the initial stage of the analysis, the target compressive load of 5 MPa was applied in different incremental steps. Then the horizontal load was applied with the constant compressive load until a target lateral displacement was achieved. The target loads were selected such that 80 and 103 % lateral deformations in the isolators were achieved.

6.5 The finite element analysis of STRP isolator

As the STRP isolator is not bonded between the superstructure and foundation beam, rollover deformation is allowed to take place in the isolator. When the rollover deformation occurs, one end of the isolator separates from the contact support while the other end is highly stressed as shown in Fig. 22a, b. To accurately simulate the STRP isolator, the size of the mesh at the corner region had to be made finer than the other areas when necessary.

The analysis is two-dimensional under the plane strain assumption. Unlike the other structural materials such as steel and concrete, deformation of the rubber is relatively severe due to its low shear modulus value. Its large deformability together with its near-incompressibility makes rubber a major challenge for FE analysis. The large deformation that the rubber components experience can only be modeled with a finite strain formulation (Kelly and Konstantinidis 2007).

FE analysis using the standard lower-order isoparametric finite elements that have not been tailored for incompressibility analysis will produce extremely poor results (Kelly and Konstantinidis 2007). More importantly, the pathological behavior called volumetric mesh-locking is likely to occur. So-called mixed methods used in modern FE analysis of incompressible and nearly incompressible materials are based on the Hellinger-Reissner and Hu-washizu variational principles (MSC Software 2010). In the mixed methods, both stress and strains are treated as unknowns (Zienkiewicz et al. 2008). The results of FE analysis presented here are based on the widely popular mixed method proposed by Herrmann (1965).

Table 5 and Fig. 22 show that the compression stress sharply increases near the corner region of the STRP isolator while the compression stress in the other areas is not significantly different but the width of the compression zone sharply decreases for increased shear strains. Due to the unbonded STRP layers, the bonding between the STRP layers is entirely dependent on the compressive stresses and friction. When compressive stresses vanish, there is always a possibility of layer separation. In Fig. 22, the region showing tensile stress is regarded to have no shear bond strength. Due to these reasons, the layer separation occurred near the top and bottom support surfaces. The strain state at different levels of shear deformation is also presented in Fig. 23.

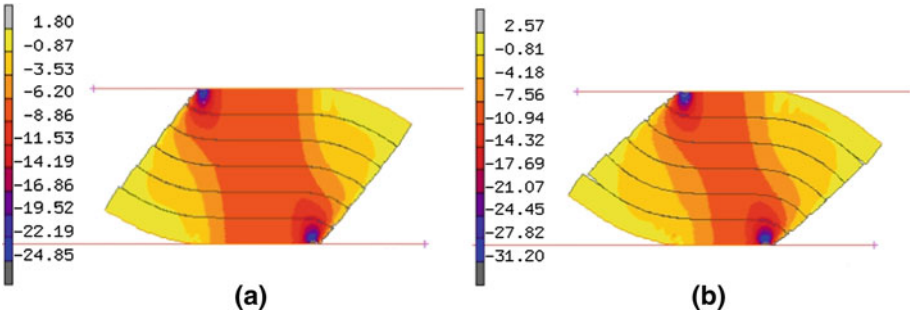

Fig. 22 Contour of normal stress S_{22} (MPa) in the rubber layers of the STRP-6 isolator. **a** 80 % shear deformation, **b** 103 % shear deformation

Table 5 Compression stress and shear bond analysis

Compression zone and stress state	Displacement					
	48 mm			62 mm		
	Top	Middle	Bottom	Top	Middle	Bottom
Compression zone width (mm)	55.0	97.48	55.0	42.48	96.26	42.48
Compression stress (MPa)	24.85	8.86	24.85	31.20	10.94	31.20

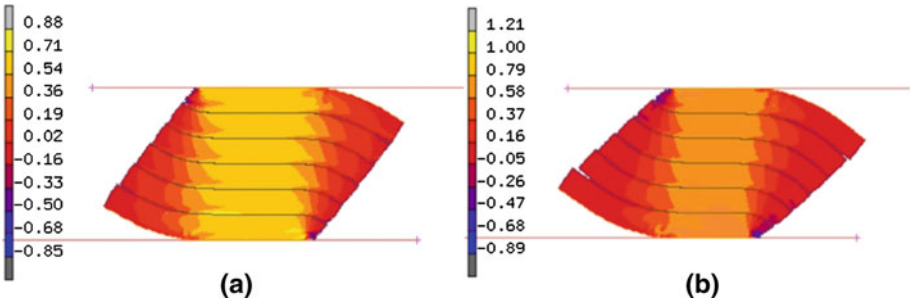

Fig. 23 Shear strain distribution within the STRP-6 isolator. **a** 80 % shear deformation, **b** 103 % shear deformation

6.6 FE analysis results and discussion

The FE analysis was carried out on the strip STRP-6 isolator whereas the experimental testing was conducted on a square STRP-6. The lateral load–displacement relationship of the STRP isolator is nonlinear as shown in Fig. 24 for both the tests and the FE analysis of STRP-6 up to 80 and 103 % lateral deformation, respectively. Due to the rollover deformation, the effective secant stiffness decreases with increased lateral deformation (Toopchi-Nezhad et al. 2011). This results in natural period elongation which further increases the efficiency of the isolator, provided that lateral stability of the STRP isolator is maintained. As seen in Fig. 24a, b, reasonable agreement is found between the experimental test and FE analysis results. However, it should be noted that for lower level lateral displacement, the horizontal force obtained by the FE analysis is noticed to be lower than the experimental results in both cases. The reason

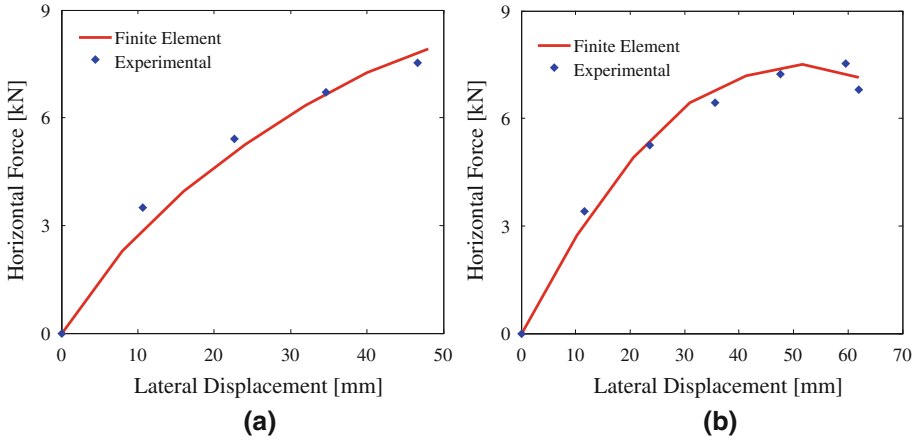

Fig. 24 Lateral load–displacement relationship of STRP-6: comparison of experimental and finite element analysis results. **a** 80 % lateral displacement, **b** 103 % lateral displacement

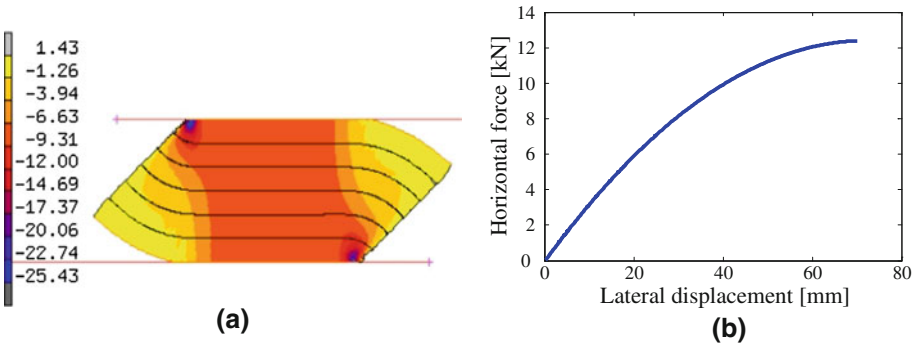

Fig. 25 150 × 150 × 72 mm STRP-6 isolator analysis result. **a** Normal stress (MPa) distribution, **b** load displacement behavior at 103 % shear strain

behind this can be the negligence of strain dependency of the steel reinforcing cords and rubber material (Toopchi-Nezhad et al. 2011).

Figure 22a, b show the distribution of normal stress in the vertical direction corresponding to 80 and 103 % lateral displacements, respectively. As shown in this figure, as a result of rollover deformation, high levels of stresses occurred at the corner region, and tensile stress is not transferred to a laterally deformed STRP at the isolator's contact supports. As a result, no balancing moment develops at the top and bottom surfaces of the STRP isolator. As seen in Fig. 22a, b, the width of the compression column zone largely decreases as the lateral displacement increases. The aspect ratio of the STRP isolator in the present case is less than two (aspect ratio = 1.39, average shape factor = 10.4) which plays an important role for the stability and stress demand of the isolator.

FE analysis of the STRP isolator with dimensions of 150 × 150 × 72 mm (aspect ratio = 2.08, shape factor = 10.4) and material properties given in Table 1 was carried out in order to investigate the effect of the aspect ratio. Constant vertical compressive load of 5 MPa was applied in order to compare the results with that of the STRP-6 isolator. Figure 25 shows the vertical compression stress as well as the horizontal force–displacement relationship. As can

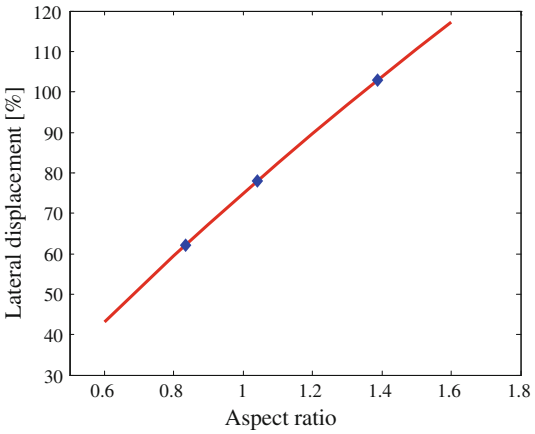

Fig. 26 Variation of maximum shear deformation capacity with aspect ratio of STRP isolator

be seen in the figure, the size of the compression column zone is wider and the maximum stresses within the isolator are also lower than the case of the $100 \times 100 \times 72$ mm size isolator shown in Fig. 22b. It also results in enhanced positive incremental force carrying capacity, which is one of the mandatory criteria for designing the seismic isolator (ASCE 2005). The aspect ratio is one of the important factors that govern the maximum shear deformation capacity of STRP isolators.

The effect of thickness on maximum shear deformation capacity of the STRP isolator is studied using the FE analysis. For this purpose, the FE analysis of eight and 10-layer STRP isolators are also carried out. In this analysis, only the thickness of isolator is increased without increasing the base dimensions. The results of the FE analysis are plotted in Fig. 26, indicating that increasing the thickness of the STRP isolator without increasing the aspect ratio sharply decreases the shear deformation capacity of the isolator.

7 Natural period of seismic isolation system

The natural period can be roughly estimated using the vertical pressure and the effective shear modulus given by Eq. (8) (Kelly 2002a,b):

$$T = 2\pi\sqrt{\frac{pt_r}{Gg}} \tag{8}$$

If the average pressure on the STRP bearing p is assumed to be 5 MPa, $G = 0.89$ MPa and $t_r = 72$ mm, the period is evaluated as 1.27 s. If the thickness is increased up to 120 mm with 10 layers, this period becomes 1.65 s. This suggests that if the period 1.65 s is acceptable as the target value for design of the isolated building structure, the STRP isolator would be adequate, provided that the vertical pressure is 5 MPa. Longer periods can be achieved by stacking more STRP layers one on top of another, although the stability of the bearing should be tested before application.

Based on the experimental test and FE analysis, it is suggested that the aspect ratio should be larger to achieve the target displacements and to attain the rollover stability. The time period mentioned here is considered as indicative value only, as the period is also related to the lateral displacements and code provisions.

8 Conclusion

This paper describes the investigation of a seismic isolation device using scrap tire rubber pads (STRP). Performance of STRP isolator with interleaved steel reinforcing cords is evaluated by means of experimental test and FE analysis. The experimental test was conducted using layer-unbonded STRP isolators which were produced by stacking the STRP layers one on top of another. The results of sample loading tests were used to calculate the different mechanical quantities of the isolator by employing established and simplified formulations. The findings obtained in this study are summarized as follows.

(1) The vertical stiffness of the STRP isolator is sufficient to withstand structural weight load of buildings as well as to prevent the rocking motion of the structure. The ratio between vertical and horizontal stiffness is greater than 150 (Eurocode 8 2004) so that the STRP isolator can be used as the base isolation device. The damping ratio of the tested STRP isolator is found to be higher than the damping ratio of the natural rubber bearing. Therefore, when using the STRP isolator for a specified level of damping, use of additional damping enhancement mechanisms can be avoided. The shear deformation capacity of the layer-unbonded STRP isolator is about 100 %, after that the layer separation occurs.
(2) FE analysis of STRP isolators is carried out on two types of samples; one with maximum lateral displacement of 80 % and the other with maximum lateral displacement of 103 %. In order to capture the accurate behavior of the STRP isolators, the hyperelastic material constants are derived by means of the uniaxial tension test of dumbbell specimens. The experimental data fitting technique is employed in order to determine the representative material constants.
(3) The finite element model is found to be almost accurate in simulating the STRP isolators as the force–displacement relationships in both the cases are in close agreement with the experimental test results. However, for lower level of lateral displacement, accuracy of the FE analysis is reduced. Due to the rollover deformation, efficiency of the isolation system increases as the lateral displacement increases.
(4) The role of the aspect ratio in rollover deformation and stability of the STRP isolator is also studied by means of FE analysis. This result suggests that the proper aspect ratio should be maintained while designing the SRTP isolator.
(5) Proper bonding between the layers is necessary as the layer separation occurred during lateral deformation. The test results and FE analysis results suggest that the STRP isolator can be used as a low cost base isolation device for ordinary residential buildings. Similar study on properly bonded STRP layers will be the focus of future investigation.

Acknowledgements The authors would like to gratefully acknowledge Prof. Aiko Furukawa of Kyoto University for her help in conducting finite element analysis and experimental tests. The authors would like to gratefully acknowledge Tokai Rubber Industries Ltd. Japan, for the assistance in the preparation of STRP samples. The authors also would like to express grateful acknowledge for the online technical support provided by the MSC Incorporation.

References

Ali A, Hosseini M, Sahari BB (2010) A review of constitutive models for rubber-like materials. Am J Eng Appl Sci 3(1):232–239

American Society of Civil Engineers (ASCE) (2005) Minimum design loads for building and other structures, ASCE Standard ASCE/SEI 7-05, Reston, VA

Eurocode 8 (2004) Design of structures for earthquake resistance-part 1: general rules, seismic actions and rules for buildings
Gerhaher U, Strauss A, Bergmeister K (2011) Numerical modeling of elastomeric bearings in structural engineering. Adv Mater Sci 11(3):51–63
Helnwein P, Liu CH, Meschke G, Mang HA (1993) A new 3-D finite element model for cord-reinforced rubber composites—application to analysis of automobile tires. Finite Elem Anal Des 14(1):1–16
Herrmann LR (1965) Elasticity equations for incompressible and nearly incompressible materials by variational theorem. AIAA J 3(10):1896–1900
Kelly JM (1999) Analysis of fiber reinforced elastomeric isolators. JSEE 2(1):19–34
Kelly JM (2002a) Analytical and experimental study of fiber-reinforced strip isolators. PEER report 2002/11. College of Engineering, University of California, Berkeley
Kelly JM (2002b) Seismic isolation system for developing countries. Earthq Spectra 18(3):385–406
Kelly JM, Konstantinidis D (2007) Low-cost seismic isolators for housing in highly-seismic developing countries. In: 10th world conference on seismic isolation, energy dissipation and active vibrations control of structures, Istanbul, Turkey
Mishra HK, Igarashi A (2012, under review) Lateral deformation capacity and stability of layer-bonded scrap tire rubber pad isolators. Bull Earthq Eng
Mordini A, Strauss A (2008) An innovative earthquake isolation system using fiber reinforced rubber bearings. Eng Struct 30(10):2739–2751
MSC Software (2010) MSC Marc Mentat, Santa Ana, CA
MSC Volume A (2010) Theory and user information, Santa Ana, CA, MSC software Corporation
MSC Volume B (2010) Element library, Santa Ana, CA, MSC software Corporation
Naeim F, Kelly JM (1999) Design of seismic isolated structures from theory to practice. Willey, London
Tomažavič M, Klemenc I, Wiss P (2009) Seismic upgrading of old masonry buildings by seismic isolation and CFRP laminates: a shaking-table study of reduced scale models. Bull Earthq Eng 7(1):293–321
Toopchi-Nezhad H, Tait MJ, Drysdale RG (2008) Testing and modeling of square carbon fiber-reinforced elastomeric seismic isolators. Structural Control and Health Monitoring 15(6):876–900
Toopchi-Nezhad H, Tait MJ, Drysdale RG (2011) Bonded versus unbonded strip fiber reinforced elastomeric isolators: finite element analysis. Compos Struct 93(2):850–859
Turer A, Özden B (2008) Seismic base isolation using low-cost scrap tire pads (STP). Mater Struct 41(5): 891–908
Uniform Building Code (UBC) (1997) Volume 2, structural design requirements, earthquake regulations for seismic isolated structure, Whittier, CA
Vossoughi J (1995) Determination of Mooney material constants for highly nonlinear isotropic incompressible materials under large elastic deformations. Exp Tech 19(2):24–27
Wong JY (2001) Theory of ground vehicle. 3. Wiley, London
Zienkiewicz OC, Taylor RL, Zhu JZ (2005) The finite element method: its basis and fundamentals, 6th edn. Butterworth-Heinemann, Oxford